A DFT study of BeX (X = S, Se, Te) semiconductor: modified Becke Johnson (mBJ) potential

© D.P. Rai*•, M.P. Ghimire+, R.K. Thapa•¶

* Beijing Computational Science Research Center, Beijing 100084, People's Republic of China
+ MANA, National Institute for Material Sciences, Tsukuba, Japan
• Dept. of Physics, Mizoram University, Aizawl, India-796004

(Получена 25 февраля 2014 г. Принята к печати 11 марта 2014 г.)

The electronic, optical and elastic properties of BeX were performed within full potential liberalized augmented plane wave method based on density functional theory (DFT). Generalized gradient approximation (GGA) and modified Becke Johnson (TB-mBJ) potential were used for exchange correlation. The mBJ gives improved band gap as compare to GGA and in close agreement with the experimental results. The present band gaps of BeS, BeSe and BeTe calculated within mBJ are 4.40, 4.0 and 2.40 eV respectively.

1. Introduction

The binary compounds BeX belong to II–VI semiconductors crystallize in four-fold coordinated zinc-blende structure [1]. These compounds are in extensive study in the recent years due to their useful physical, electro-optical and other properties [2–4]. The distinguish features of beryllium chalcogenides are small ionic radius ratio and the high degree of covalent binding. The ionicities range from 0.169 in BeTe to 0.312 in BeS [5]. Furthermore, Be-monochalcogenides are semiconductors with indirect band gap along $\Gamma-X$ symmetry. They have large band gaps (2.7–5.5 eV) and a high value of the bulk modulus which results in an increased hardness and stability [6]. These interesting properties make them potentially useful for technological applications. These materials have been studied by many methods within different approximations to reproduce the accurate description of electronic properties. The first theoretical study of Be-chalcogenides was done by Stukel [7], used the selfconsistent orthogonalized-plane wave method (SCOPW) within the non-relativistic Slaters local approximation to calculate the band structure and the dielectric function of BeX. Sarkar and Chatterjee [8] studied the band structure using the composite wave variational version of the augmented plane wave method (APW) in conjunction with the linear combination of atomic orbitals (LCAO) method. Gonzalez Díaz et al. [9] and Munoz et al. [10] employed the first-principles pseudo potential (PP) method based on the density functional formalism to study the structural phase transition of these compounds. The structural and electronic properties of BeX compounds have also been investigated by Kalpana et al. [11] using the tight binding linear muffin tin orbitals (FP-LMTO). Fleszar and Hanke [12] have studied the electronic excitations of BeS, BeSe and BeTe by means of the ab initio GW-approach. The elastic constants of BeSe and BeTe have been calculated by Doyen-Lang et al. [13], using the De Launay model (DLM) based on atomic model and angular central forces. The experimental results of these compounds are very few because of their high toxic nature which makes it difficult to obtain as a single crystal or epitaxial layers [14–16].

In most of the semiconductors the theoretical (LDA/GGA) [17] energy band gaps are underestimated as compared to the experimental results. Thus further approximations are required to modify the results in order to make it comparable with the experimental one. As proposed by Aryasetiawan et al. the most appropriate tool to study the band gap is the many body perturbation theory, within the GW approximation [18] but this theory is computationally expensive. The theoretical band gap differs from the experimental by a factor called derivative discontinuity (Δ_{xc}) [19]. Tran and Blaha gave an alternative method which is computationally cheap and equally efficient in band gap calculations, by modifying the Becke Roussel exchange potential $v_{x,\sigma}^{BR}$ [20] which is created by exchange hole. The modified Becke–Johnson (mBJ) potential [21] read as

$$v_{x,\sigma}^{mBJ}(r) = c v_{x,\sigma}^{BR}(r) + (3c-2)\frac{1}{\pi}\sqrt{\frac{5}{6}}\sqrt{\frac{t_\sigma(r)}{\rho_\sigma(r)}}, \qquad (1)$$

which is the response of the exchange hole potential to density variation containing derivative discontinuity Δ_{xc}. In Eq. (1) $\rho_\sigma(r) = \sum_{i=1}^{N_0} |\psi_{i,\sigma}|^2$ is the electron density, $t_\sigma(r) = 1/2\sum_{i=1}^{N_0} \nabla\psi_{i,\sigma}^*$ is the kinetic energy density and $\sqrt{\frac{t_\sigma(r)}{\rho_\sigma(r)}}$ can be considered as screening term. An Eq. (1) is written in such a way that for any value of c the exchange potential is obtained for constant electron density.

$$c = \alpha + \beta\left(\frac{1}{V_{\text{cell}}}\int_{\text{cell}}\frac{|\nabla\rho(r')|}{\rho(r')}\,d^3r\right)^{1/2} \qquad (2)$$

where V_{cell} is the unit cell volume, α and β are two free parameters whose values are $\alpha = -0.012$ and $\beta = 1.023$

¶ E-mail: dibyaprakashrai@gmail.com

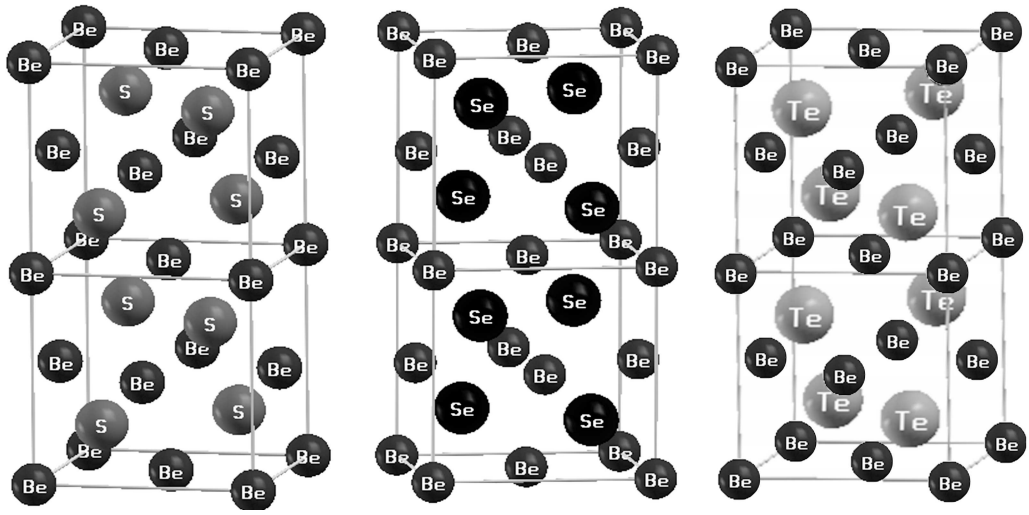

Figure 1. Crystal structure of BeX.

bohr$^{1/2}$ according to a fit to experimental results [22]. There are many results of improved band gap within TB-mBJ. Yousaf et al. studied the X-Phosphides (X = B, Al, Ga, In) III–V type semiconductors using mBJ and reported the improved band gap over LDA/GGA [23]. III-nitride semiconductors considering zinc blende and wurtzite crystal structures with TB-mBJ yields an excellent agreement with the experimental results [24]. Guo and Liu studied the zinc blende transition metal compounds using mBJ and reported the increased half metallic (HM) gap with respect to GGA/LDA [25]. The similar explanation of improved band gap within mBJ was found in topological half-Heusler (THH) compounds [26] as well.

Presently, many calculations of the band structures have been reported for these compounds with underestimated band gap as compared to experimental one. But there are few reports on the band structures of BeX with exact band gap. To sort out this discrepancy we have used new exchange correlation functional modified Becke Johnson (mBJ) potential within a frame work of DFT. The aim of this work is to give a detailed description of the behaviour of electronic, optical and elastic properties of the zinc blende BeX.

2. Computational details

Experimental lattice constants were used for volume optimization to obtain the optimized lattice parameters. The ground state calculation based on full potential linearized augmented plane wave (FPLAPW) method as implemented in WIEN2K [27] package has been employed to perform the self-consistent electronic structure calculations. Both LDA/GGA [17] and mBJ has been used for exchange correlations. Nonspherical contributions to the charge density and potential within the muffin tin (MT) spheres were considered up to $l_{\max} = 10$ (the highest value of angular momentum functions). The cut-off parameter was $R_{\mathrm{MT}} \times K_{\max} = 8$ where $K_{\max}$ is the maximum value of the reciprocal lattice vector in the plane wave expansion and R_{MT} is the smallest atomic sphere radii of all atomic spheres. In the interstitial region the charge density and the potential were expanded as a Fourier series with wave vectors up to $G_{\max} = 12$ arb. units. The number of k-points used in the irreducible part of Brillouin zone is 286. The mesh of 1000k points was taken to perform the Brillouin zone integration and the self-consistency convergence is 10^{-3} Ry. The details of R_{MT} of BeX compounds are given in Table 1.

Table 1. R_{MT} [arb. units]

Compounds	Muffin Tin Radius (RMT) arb. units	
	Be	X
BeS	1.99	1.99
BeSe	2.11	2.11
BeTe	2.30	2.30

3. Crystal Structure

Beryllium monochalcogenides BeX (X=S, Se, Te) crystallizes in zinc-blende structure. BeX contains two atoms that form fcc primitive crystal with space group F-43m. The Wyckoff positions positions are at Be (0, 0, 0) and X(1/4, 1/4, 1/4). The unit cell structure of BeX is presented in Fig. 1.

4. Electronic properties

The fitting of the Murnaghan equation of state [28] to the total energy versus volume yields to the equilibrium

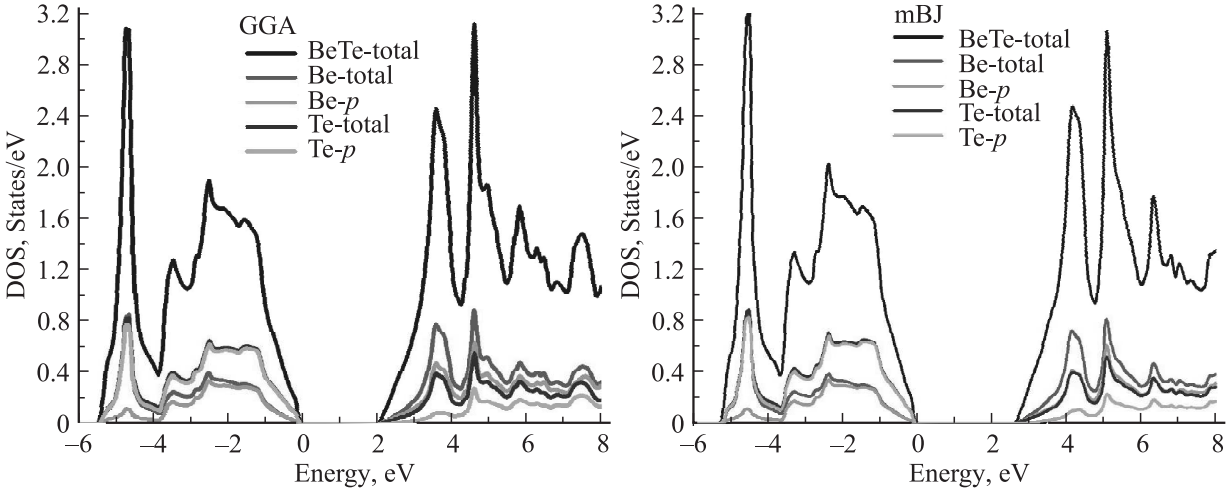

Figure 2. Total and partial DOS of BeTe.

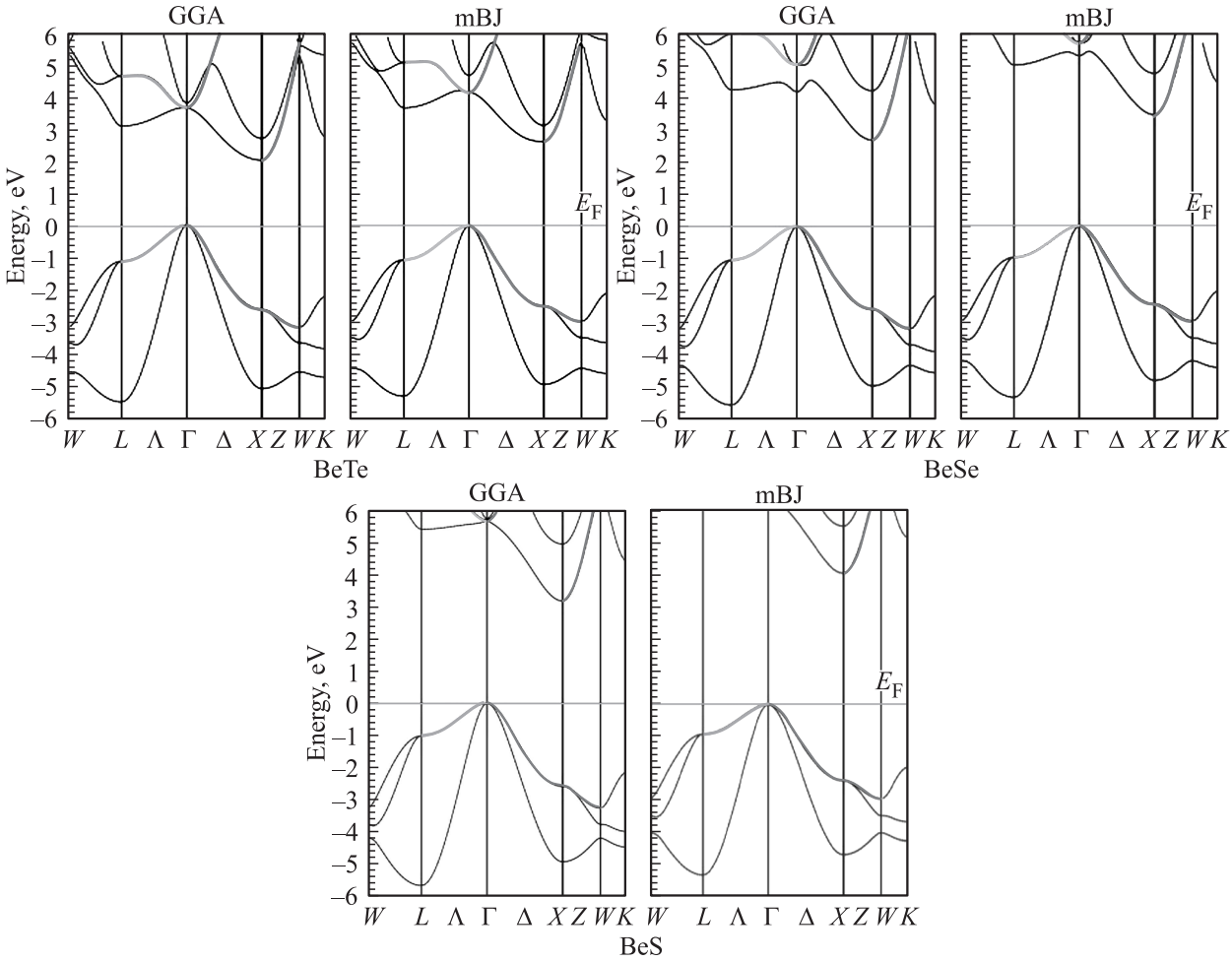

Figure 3. Band structures of BeS, BeSe and BeTe calculated within GGA and mBJ.

lattice constant (a_0) and the bulk moudulus (B) presented in Table 4. The electronic structures were calculated with the stable lattice constant. The total DOS along with the partial DOS and band structures of BeX calculated with GGA and mBJ are shown in Figs. 2, 3. BeS, BeSe and BeTe have the similar electronic structure within GGA and mBJ thus only DOS plot of BeTe is presented in Fig 2. The Fermi energy is set at 0 eV. The distinct features

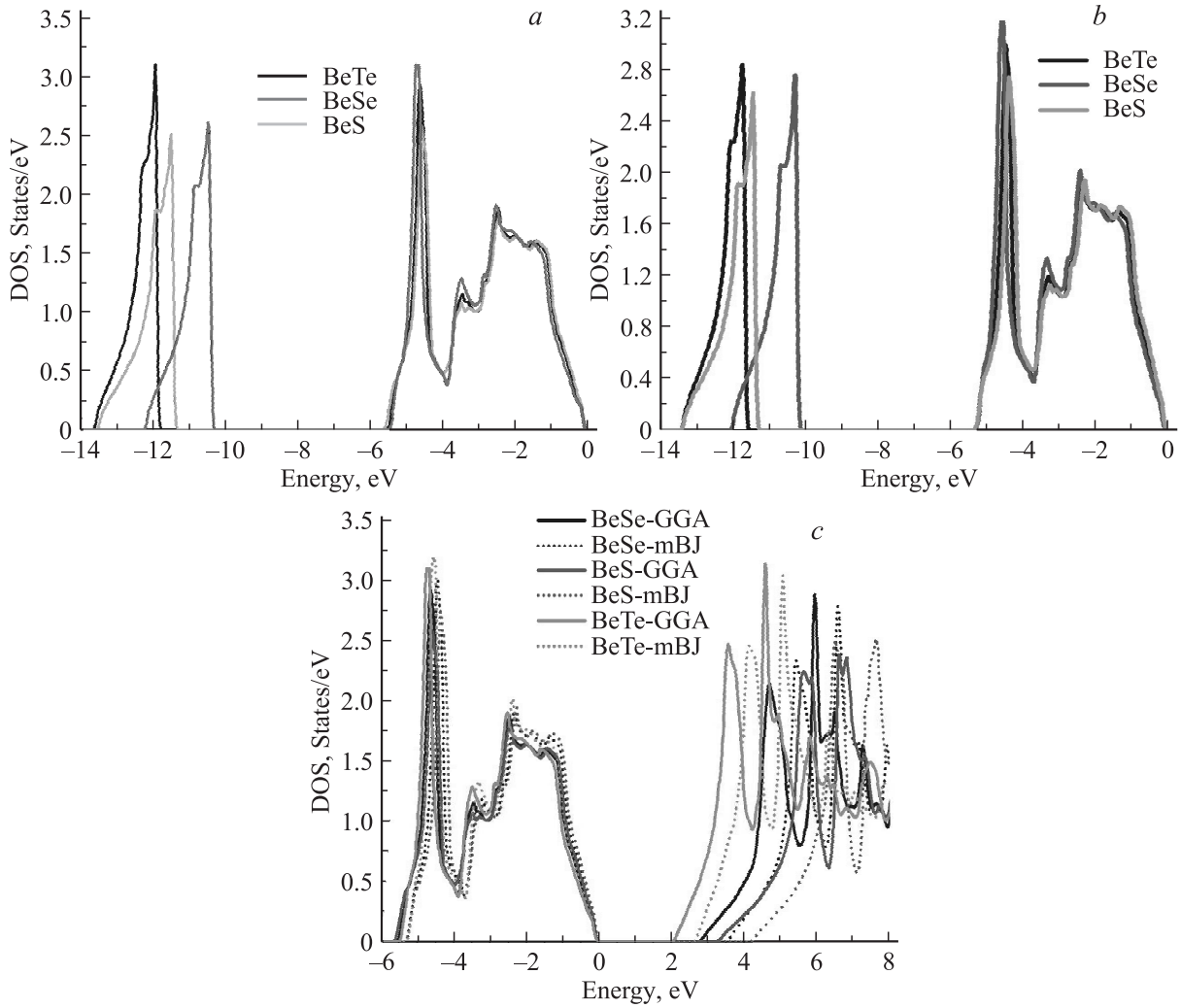

Figure 4. *a, b* valence band width and (*c*) comparison of band gaps of BeX (GGA & mBJ).

noticed within mBJ as compared to GGA is shifting of the conduction band and wide opening of the band gaps. We have observed that the chalcogen *p*-band in the conduction region shifted up in the energy level while going from telluride to sulphide. The shifting of *p*-band was due to the increase in the lattice parameters as explained by Wei et al. for II–VI compounds [29]. The contribution from the *s* states to total DOS is neglected as it is very small and not presented in the Fig. 2. In all cases the top of the valence band maxima (VBM) and the conduction band minima (CBM) occur at Γ and *X* point respectively as shown in Fig. 3. Thus the energy gap is an indirect band gap between VBM and CBM. The comparison of band gaps of BeX calculated withing GGA and mBJ are displayed in Fig. 4, *c*. The order of the band gaps are given as $E_g(\mathrm{BeS}) > E_g(\mathrm{BeSe}) > E_g(\mathrm{BeTe})$. The overall band gap results of GGA are found to be in fair agreement with the previous theoretical results (LDA, TB-LMTO, SCOPW, LCAO) but significantly underestimated from the experimental values as shown in Table 2. Whereas the implementation of new exchange-correlation functional called mBJ potential has resolved this discrepancy of band gap and provided an almost exact value as compared to experimental data (Table 2). In all the systems the CBM has been shifted towards the higher energy as compared to GGA position but the position of VBM is shifted least, almost fixed at the GGA position. Mostly the unoccupied band has been shifted upward from the Fermi level which results an increase in the band gap within mBJ. The upper VBM nearby Fermi level are dominated by the *p* states

Table 2. Energy gap calculated within GGA and mBJ

Compound	GGA	mBJ	Previous	Expt.
BeS	3.30	4.40	3.13[a]/4.17[c]	5.50[b]
BeSe	2.70	4.00	2.63[a]/3.61[c]	4.50[b]
BeTe	2.10	2.40	1.98[a]/2.50[d]	2.70[b]

Note. [a]Ref. [1], [b]Ref. [14], [c]Ref. [7], [d]Ref. [12].

of the chalcogen atoms in BeS, BeSe and BeTe. The conduction band is composed of p states as majority contribution from Be-p states. An analysis of the p band in the valence region gives the width of the valence band ($-5.5-0.0$ eV). From Fig. 4, *a* the energy range from 0.0 to -13.70 eV represents the band widths of BeX in the valence region within GGA. The calculated band widths are 13.40, 13.70 and 12.20 eV for BeS, BeSe and BeSe respectively which agrees well with the previous studies at 0 pressures [1]. The valence band below -10.00 eV (core region) is mostly formed by the s states of chalcogen. The valence band width (VBW) is maximum for BeSe (13.70 eV). Within mBJ the minima of the s band for BeSe and BeS are in the equal footing as shown in Fig. 4, *b*. Indicating that the wave function is more localized going from BeTe to BeS. As the atomic number of an anion decreases the indirect band gap increases, implies that the materials become less covalent and more ionic [30]. This contradicts our results presented in section 6 which favours BeTe to be more ionic. The band gap between the lowest band (anion s band) and the valence band due to p states calculated within GGA are 5.80, 6.20 and 4.90 eV for BeS, BeSe and BeTe respectively (Fig. 4, *a*). The $s-p$ band gap is lowest for BeTe due to the higher energy position of Te-s band (Figs. 4, *a, b*). The results of the dependency of VBW on hydrostatic pressure reported that VBW increases with increasing pressure which results in decrease of ionicity [30].

5. Optical Properties

Dielectric function $\varepsilon(\omega)$ of the electron gas depending on the frequency has some important role in determining the physical properties of solids. It has two parts real and imaginary [31]

$$\varepsilon(\omega) = \varepsilon_1(\omega) + i\varepsilon_2(\omega). \tag{3}$$

The imaginary part of the complex function $\varepsilon_2(\omega)$ in cubic symmetry compounds can be calculated by relation [32]

$$\varepsilon_2(\omega) = \frac{8}{2\pi\omega^2} \sum_{nn'} \int_{BZ} |Pnn'(k)|^2 \frac{dS_k}{\nabla\omega_{nn'}(k)}, \tag{4}$$

where $\omega_{nn'}$ is the joint density of states and $P_{nn'}$ is momentum matrix. Kramers–Kronig relation gives the real part of the complex dielectric function $\varepsilon_1(\omega)$ [33]

$$\varepsilon_1(\omega) = 1 + \frac{2}{\pi} P \int_{\infty}^{\infty} \frac{\omega'\varepsilon_2(\omega')}{\omega'^2 - \omega^2} d\omega. \tag{5}$$

The values of the real and imaginary part of the dielectric function provide the basis for the refractive index $\tilde{n}(\omega)$. The complex refractive index is

$$\tilde{n}(\omega) = n(\omega) + ik(\omega) = \varepsilon^{1/2} = (\varepsilon_1 + \varepsilon_2)^{1/2}, \tag{6}$$

where $n(\omega)$ and $k(\omega)$ are the real and imaginary part (extinction coefficient) of the refractive index:

$$n(\omega) = \frac{1}{\sqrt{2}} \left[\{\varepsilon_1(\omega)^2 + \varepsilon_2(\omega)^2\}^{1/2} + \varepsilon_1(\omega)\right]^{1/2}, \tag{7}$$

$$k(\omega) = \frac{1}{\sqrt{2}} \left[\{\varepsilon_1(\omega)^2 + \varepsilon_2(\omega)^2\}^{1/2} - \varepsilon_1(\omega)\right]^{1/2}. \tag{8}$$

If the medium is very weakly absorbing then we can assume $k(\omega)$ is very small, so that

$$n = \sqrt{\varepsilon}, \qquad k = \frac{\varepsilon_2}{2n}.$$

These equations tells that refractive index is related with real part and absorption coefficient $[\alpha(\omega)]$ is related with the imaginary part of dielectric function. It is not valid for the case when the medium has large absorption coefficient [34]

$$\alpha(\omega) = 2\omega k(\omega) = \sqrt{2}\omega \left[\{\varepsilon_1(\omega)^2 + \varepsilon_2(\omega)^2\}^{1/2} - \varepsilon_1(\omega)\right]^{1/2}. \tag{9}$$

Similarly the absorption coefficient can be calculated from Beer's Law is

$$\alpha = \frac{2k\omega}{c} = \frac{4\pi k}{c}.$$

Reflectivity can be calculated as

$$R(\omega) = \left|\frac{\tilde{n} - 1}{\tilde{n} + 1}\right| = \frac{(n-1)^2 + k^2}{(n+1)^2 + k^2}. \tag{10}$$

While the electron energy loss function [34] is given by

$$lm\left(\frac{1}{\varepsilon}\right) = -\varepsilon_2/(\varepsilon_1^2 + \varepsilon_2^2). \tag{11}$$

The reflectivity, refractive index (real and imaginary), dielectric function (real and imaginary), electron energy loss function and optical conductivity calculated within GGA and mBJ are shown in Figs. 7, 8. The real and imaginary part of dielectric function is calculated in the energy range $0-14$ eV within GGA and mBJ as shown in Fig. 7. Transition from the top of the valence bands to conduction bands contribute to optical spectra. The onset of absorption edge in ε_2 occurs at 3.2, 4.0 and 5.2 eV for BeTe, BeSe and BeS respectively within GGA. Similarly within mBJ the transition occurs at higher energy 4.0, 5.0 and 6.5 eV for BeTe, BeSe and BeS respectively. BeTe, BeSe and BeS have strong absorption in between the energy range (4.5–8.0), (5.5–10.0) and (6.5–12.0) eV respectively within mBJ. This region is represented by different peaks due to electronic transition between the valence and conduction band ($\Gamma_v - \Gamma_c$). The static ε_1 ($\omega = 0.0$ Hz) and low $\varepsilon_1(\omega)$ are strongly depend on the semiconductor's band gap. Penn model relating the inverse relation with band gap E_g [35]

$$\varepsilon_1(0) \approx 1 + (\hbar\omega_p/E_g)^2 \tag{12}$$

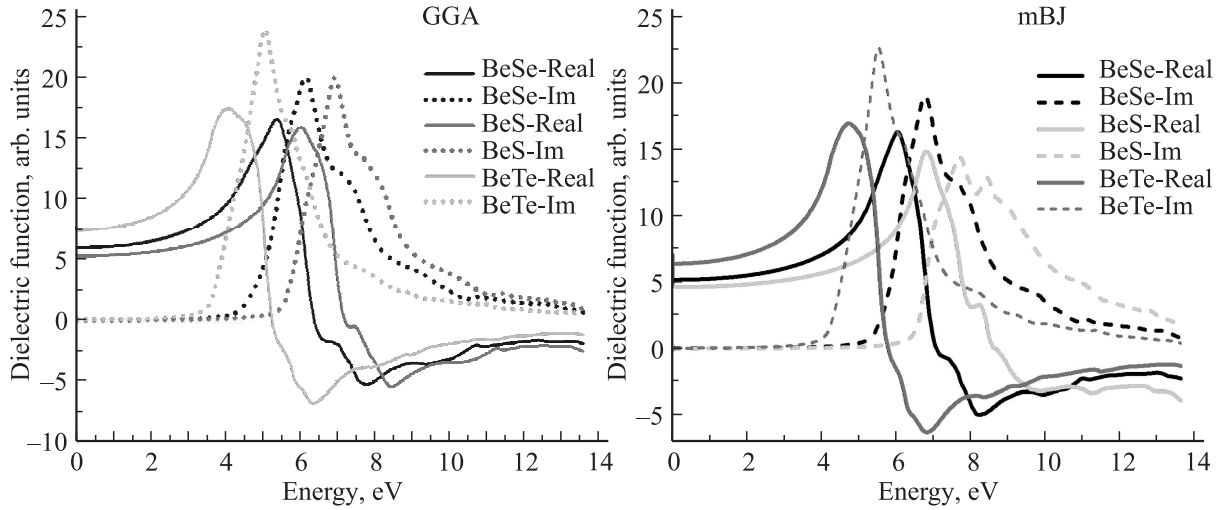

Figure 5. Real and imaginary part of dielectric function of BeX (GGA & mBJ).

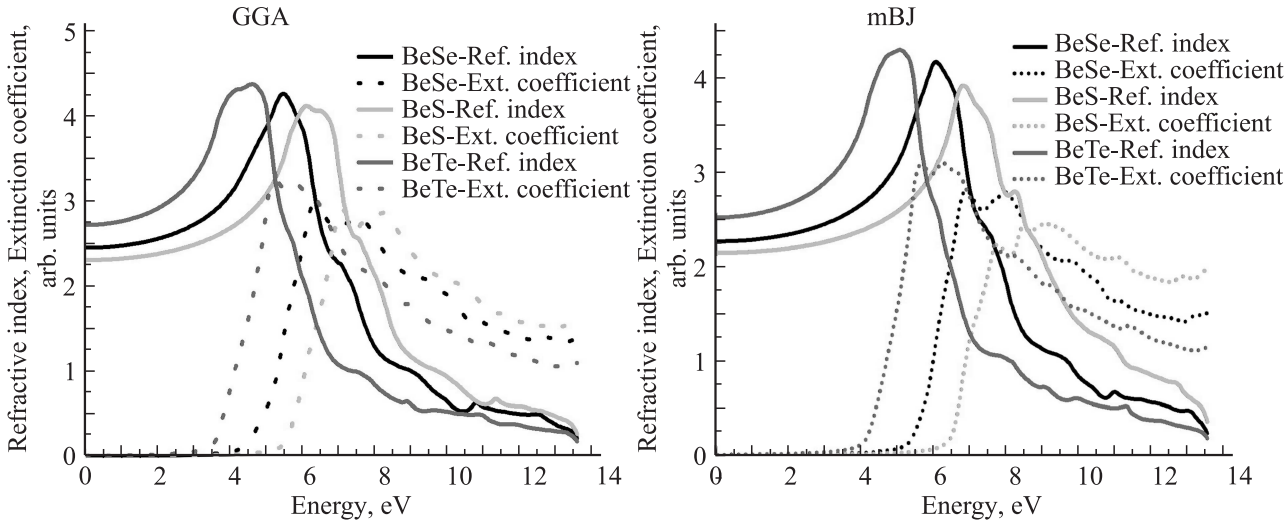

Figure 6. Refractive index and extinction coefficient of BeX (GGA & mBJ).

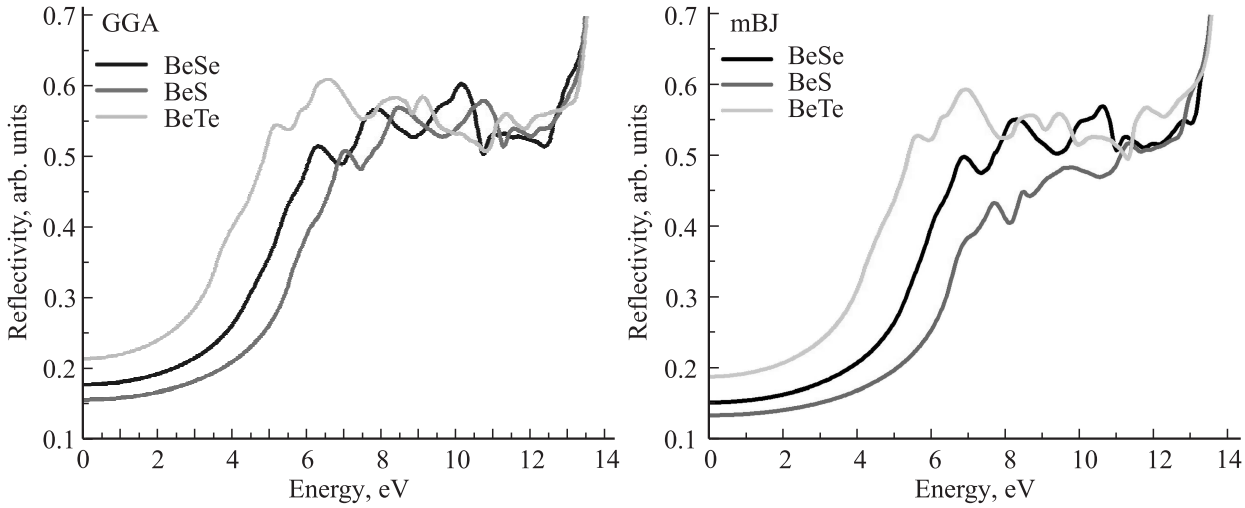

Figure 7. Reflectivity of BeX (GGA & mBJ).

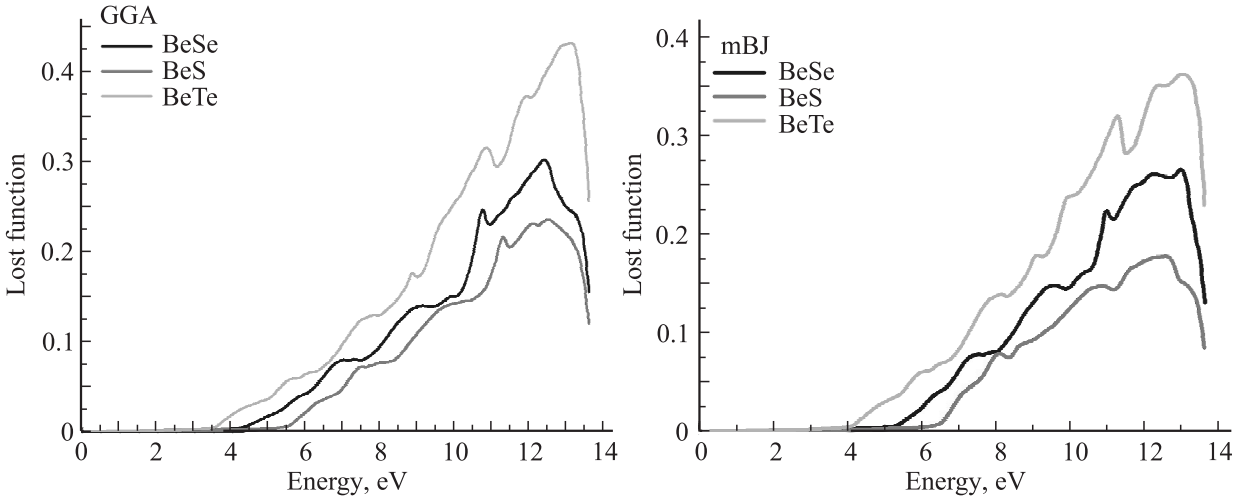

Figure 8. Optical conductivity of BeX (GGA & mBJ).

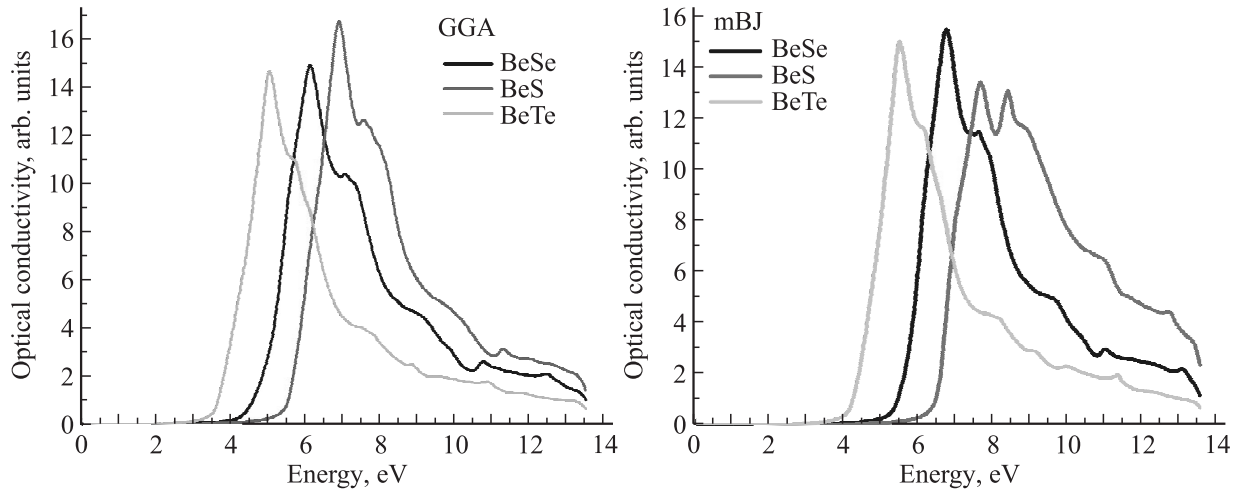

Figure 9. Optical conductivity of BeX (GGA & mBJ).

where $\hbar\omega_p$ is the plasma energy. With mBJ it is clear from Fig. 5 that ε_1 initially increases up to maximum at 5.00, 6.30 and 7.0 eV and decreases to zero at 6.0, 7.0 and 8.5 eV for BeTe, BeSe and BeS respectively. The values of ε_1 lower than 1 unit exhibit the reflectiveness of the material indicating a metallic character. So these materials can be used as a protection from radiation in this energy range (ultra violet radiation). The negative $\varepsilon_1(\omega)$ is stable after 10 eV which suggests that the materials do not interact with high energy photons and remain transparent thus suitable for optical lenses. Fig. 6 shows the refractive index and extinction coefficient calculated within GGA and mBJ. The index $n(\omega)$ closely follows the $\varepsilon_1(\omega)$. The values of $n(\omega)$ reaches maximum at 5.0, 6.5 and 7.8 eV for BeTe, BeSe and BeS respectively within mBJ. The spectrum of $n(\omega)$ falls of and vanishes at the higher energies as the materials absorb high energy photons and transparency is lost. The refractive index above photon energy 7.0, 9.5 and 11.0 eV for BeTe, BeSe and BeS respectively (see Fig. 6) decreases below unity which indicates the phase velocity of light is greater than the light celerity c, which is contradictory to relativity [34]. As the phase velocity is given by $v = \frac{\omega}{k} = \frac{c}{n}$. However the fact is that a signal transmitted as a wave packet (group velocity, $v_g = \frac{d\omega}{dk}$) rather than a monochromatic wave (phase velocity) in a dispersive medium. The relationship between group and phase velocity is given as $v_g = v\left(1 - \frac{k}{n}\frac{dn}{dk}\right)$.

The extinction coefficient $k(\omega)$ closely follows the $\varepsilon_2(\omega)$ compare Figs. 5, 6. A variation of $k(\omega)$ from $\varepsilon_2(\omega)$ is attributed to small optical conductivity [34]. Fig. 7 shows the reflectivity curve with respect to photon energy. The reflectivity spectrum is small in the low energy region indicating that inter band transition do not occur in the infrared spectrum. The inter band transition for BeTe, BeSe and BeS occurs above 5.0, 7.0 and 7.7 eV respectively within mBJ which makes these compounds applicable in visible and ultra violet region. It has been observed in Fig. 7,

Table 3

	Reflectivity		Refractive index		Dielectric fn. (ε_1)			ω_p ($\times 10^{14}$ Hz)	
	GGA	mBJ	GGA	mBJ	GGA	mBJ	Other	GGA	mBJ
BeTe	0.22	0.19	2.75	2.60	7.50	6.00	7.597[a]/6.9[b]	81.341	91.724
BeSe	0.18	0.15	2.50	2.30	6.25	5.00	6.334[a]/6.1[c]	93.989	124.58
BeS	0.16	0.13	2.25	2.20	5.50	4.50	5.806[a]	106.354	134.27

Note. [a]Ref. [30], [b]Ref. [36], [c]Ref. [37]

for high energy photons reflectivity is maximum and then stabilizes up to some energy value. This behavior is due to the fact that the semiconducting behavior is lost and metallic character predominates. The electron energy loss-function of BeX calculated within GGA and mBJ are displayed in Fig. 8. The order of loss function on the basis of width and height of the peaks are given as BeTe > BeSe > BeS. It is obvious from Fig. 8 that for a photon with energy lesser than the band gap of a material, no energy loss occurs which means no scattering of electrons. Obviously mBJ gives an energy loss at high energy range as compared to GGA as the band gap is large. The slow rise in the slope of energy loss is due to inelastic scattering, it increases with increasing energy. The peaks in the energy loss spectrum correspond to plasma resonance. These materials exhibit metallic behavior above peak value whereas below peak values they show dielectric property [30]. The optical conductivity curve is shown in Fig. 9. The range of optical conductivity within mBJ for BeTe, BeSe and BeS are 4–10, 5.5–11 and 6.5–13 eV respectively. Among BeTe and BeSe, BeS shows the highest optical conductivity peak within GGA which agrees well with the previous reported result (LDA) [1] this is contrary to the present mBJ result. The optical conductivity is highest for BeSe within mBJ as shown in Fig. 9. The static reflectivity, refractive index, real part of dielectric constant (ε_1) and plasma frequency (ω_p) calculated from Eq. 12 are tabulated in Table 3.

6. Elastic properties

As one can observe that C_{11}, C_{12}, C_{44} values satisfy the condition $(C_{11} - C_{12}) > 0$, $(C_{11} + 2C_{12}) > 0$, $C_{11} > 0$, $C_{44} > 0$, cubic stability. Thus the structure of BeX is mechanically stable. The elastic anisotropy of crystals has an important implication in engineering science since it is highly correlated with the possibility to induce micro cracks in materials [38]. To quantify the elastic anisotropy of these compounds, we have computed the anisotropy factor. A from the present values of the elastic constants. For a completely isotropic material, $A = 1.0$, while any value smaller or larger than1 indicates anisotropy. The magnitude of the deviation from 1 is a measure of the degree of elastic anisotropy possessed by the crystal. The Zener anisotropy factor $(A = \frac{2C_{44}}{C_{11}-C_{12}})$, Poisson's ratio $(\gamma = \frac{3B-2G_H}{2(3B+2G_H)})$, Shear modulus $(C' = 1/2(C_{11} - C_{12}))$, Bulk modulus $(B = \frac{1}{3}(C_{11} + 2C_{12}))$ which represents the resistance to volume change and Young modulus $(Y = \frac{9BG_H}{3B+G_H})$ [39] are calculated within GGA, where $G_H = \frac{G_R+G_V}{2}$ is the isotropic shear modulus, G_V is Voigt's shear modulus [40] and G_R is Reuss's shear modulus [41] presented as:

$$G_V = \frac{C_{11} - C_{12} + 3C_{44}}{5}$$

and

$$G_R = \frac{5(C_{11} - C_{12})C_{44}}{4C_{44} + 3(C_{11} - C_{12})}.$$

The Kleinman parameter (ξ) [42] describes the relative positions of the cation and anion sub-lattices under volume conserving strain distortions, for which positions are fixed by symmetry. We use the relation: $\xi = \frac{C_{11}+8C_{12}}{7C_{11}+2C_{12}}$. The calculated values of Bulk Modulus (B), Poisson's ratio (γ), Shear modulus (C'), Young modulus (Y), isotropic

Table 4 (units in GPa)

	a_0(Å)	B	C_{11}	C_{12}	C_{44}	ξ
BeS						
Present(GGA)	5.040	64.079	121.34	34.446	65.929	0.430
Expt.[a]	4.870	105.00				
LDA[b]	4.800	100.80	167.00	68.000	105.00	0.544
FP-LAPW[c]	4.803	103.70	143.70	84.000	91.10	
TB-LMTO[d]	4.839	102.80	140.32	95.950	23.89	
PP[e]	4.745	116.00	184.00	75.000	99.00	0.420
BeSe						
Present	5.429	41.567	83.270	20.716	50.753	0.399
Expt.[f]	5.137	92.200				
LDA[b]	5.093	82.450	153.00	56.00	88.00	0.508
FP-LAPW[c]	5.084	86.080	151.70	53.30	53.70	
TB-LMTO[d]	5.089	89.280	113.10	77.36	19.38	
PP[e]	5.037	98.000	149.00	59.00	81.00	0.43
DLM[g]	5.037		149.70	82.40	40.20	
BeTe						
Present	5.796	41.208	52.142	35.741	31.623	0.793
Expt.[a]	5.617	66.800				
LDA[b]	5.581	62.360	99.000	44.000	68.000	0.77
FP-LAPW[c]	5.556	64.900	104.20	44.000	53.400	
TB-LMTO[d]	5.563	68.48	85.56	59.94	13.600	
PP[e]	5.531	70.60	111.00	43.00	60.00	0.44
DLM[g]	5.626		86.30	56.80	20.70	

Note. [a]Ref. [52], [b]Ref. [1], [c]Ref. [53], [d]Ref. [30], [e]Ref. [9], [f]Ref. [54], [g]Ref. [13].

Table 5 (units in GPa)

Compound	A	C'	G_R	G_V	G_H	γ	Y	B/G_H	H_v
BeS	1.517	43.447	54.623	56.936	55.780	0.030	129.70	1.149	8.423
BeSe	1.623	31.277	40.633	42.963	41.798	0.098	93.915	0.995	6.312
BeTe	3.856	8.202	14.762	22.2546	18.508	0.269	48.294	2.226	2.795

Table 6. Mass (M in g/mol), v_l, v_t, v_m (in m/s), Debye temperature (θ_D in K) and density (ρ)[g/cm^3]

Compound	Volume (Å^3)	Mass	Density (ρ)	v_t	v_l	v_m	θ_D
BeS	32.054	41.077	1.279	6603.333	10403.372	13765.795	1372.592
BeSe	39.987	87.972	2.220	4358.795	6620.255	20951.260	1947.732
BeTe	48.629	136.612	2.809	2566.870	4843.045	34857.402	3026.673

shear modulus(G_H), Voigt's shear modulus (G_v), Kleinman parameter (ξ) are presented in Table 4, 5. The unit GPa has been used throughout the text for the calculation of elastic constants. Poisson's ratio is the measure of compressibility, interestingly, as $\gamma \to 1/2$, material tends to incompressibility [43] and at $\gamma = 1/2$ the material is nearly incompressible. The value of the Poisson ratio (γ) for covalent materials is small (0.1), whereas for ionic materials a typical value of γ is 0.25 [44]. Frantsevich et al. suggested that the Poisson's ratio can be used as an indicator for ductile ($\gamma > 1/3$) or brittle behavior ($\gamma < 1/3$) [45]. Another criterion for ductility or brittleness is the value of the B/G_H ratio. The higher or lower the B/G_H ratio is, the more ductile or brittle the material respectively. The critical value which separates ductile and brittle materials is approximately [1.75] [46]. The calculated γ for BeS, BeSe and BeTe are 0.03, 0.098 and 0.269 respectively, thus it can be predicted that BeTe is ionic where as BeSe is covalent as shown in Table 5. B/G_H ratio is 2.226 for BeTe higher than 1.75 which indicates more ductility in nature as compare to BeS and BeSe. The calculated anisotropy factor is 3.856 in BeTe highest among BeSe and BeS. As the atoms along the edge of FCC crystal is more separated than along the face diagonal. This causes anisotropy in the system. BeTe gives high anisotropy with high γ value and high B/G_H ratio as compare to BeS and BeSe. It has been suggested that the intrinsic correlation between hardness and elasticity of materials correctly predicts Vicker's hardness for a wide variety of crystalline materials as well as bulk metallic glasses (BMGs) [47]. If a material is intrinsically brittle, its Vicker's hardness linearly correlates with the shear modulus ($H_v = 0.151G_H$) [48]. The calculated value of Vicker's hardness for BeS, BeSe and BeTe are 8.423, 6.312 and 2.795 GPa respectively (see Table 5).

The Cauchy pressure relation $C_{12}-C_{44}$, can be used to characterize the bonding type [49]. Negative Cauchy pressure corresponds to more directional bonding, while positive values indicate predominant metallic bonding. In our calculation BeS and BeSe gives the negative value of Cauchy pressure, indicates directional bonding whereas metallic bond predominates in BeTe. Higher values of Young's modulus (γ) in comparison to the bulk modulus (B) (see Table 4, 5) indicate the material is hard to break [50]. The calculated ξ for BeS and BeSe agrees well with the previous results calculated within pseudo potential method (PP) [9] except for BeTe. The condition for structural and cubic stability has given by the relation $C_{12} < B < C_{11}$ [51], which give credence to our result.

The Debye temperature (θ_D in K) is a fundamental physical property, and is used to distinguish between high-and low temperature regions for a solid. At low temperature ($T < \theta_D$) one expects high-frequency modes to be frozen, the vibrational excitations arise solely from acoustic vibrations and θ_D calculated from elastic constants is same as that determined from specific heat measurement. If ($T > \theta_D$) we expect all modes to have energy k_BT [55]. In the present case, Debye temperature (θ_D) is estimated for BeS, BeSe and BeTe for ($T < \theta_D$) by using the calculated elastic constant data, in terms of the following classical relations [39].

$$\theta_D = \frac{h}{k}\left[\frac{3n}{4\pi}\left(\frac{N_a\rho}{M}\right)\right]^{\frac{1}{3}} v_m,$$

where v_m is the average wave velocity, h is Planck's constants, k is Boltzmann's constant, N_a is Avogadro's number, n is the number of atoms per formula unit, M is the molecular mass per formula unit, $\rho = M/V$ is the density, and v_m is obtained from [56]:

$$v_m = \left[\frac{1}{3}\left(\frac{3}{v_t^3} + \frac{1}{v_l^3}\right)\right]^{-1/3},$$

where v_l and v_t are the longitudinal and transverse elastic wave velocities respectively, which are obtained from Navier's equations [57]

$$v_l = \left(\frac{3B + 4G_H}{3\rho}\right)^{1/2} \text{ and } v_t = \left(\frac{G_H}{\rho}\right)^{1/2}.$$

The calculated average longitudinal and transverse elastic wave velocities and Debye temperature for BeS, BeSe and

BeTe are given in Table 6. As we have not found any experimental data to compare our result of these properties in the literature for these compounds. Future experimental work may testify our calculated results.

7. Conclusion

The electronic band structures, optical and elastic properties of BeS, BeSe and BeTe are investigated using the FP-LAPW method. The binary Be-monochalcogenides are indirect band gap compounds and are optically inactive. The band gaps calculated within GGA are underestimated as compared to experimental one. This discrepancy has been solved by opting a new exchange correlation functional, modified Becke Johnson (mBJ) potential within a frame work of DFT. The calculated band gaps within mBJ ar 4.40, 4.00 and 2.40 eV for BeS, BeSe and BeTe respectively which are in close agreement to experimental results. Our study of elastic properties have revealed that BeS is predicted to be a hardest material with largest value of Young's modulus 129.70 GPa and Vicker's hardness factor 8.423 GPa. The calculated Possion's ratio (0.269) close to 0.25 and the highest value of B/G_H (2.226) in BeTe suggests that this material is compressible and ductile in nature. Cauchy pressure relation predicted metallic bonding in BeTe. BeSe is more covalent in nature with $\gamma = 0.098$ close to 0.10. The optical properties like dielectric functions, refractive index, energy loss function, reflectivity, optical conductivity are also calculated. These parameters are inter related and band gap dependent. Furthermore, it is suggested that these materials need to be studied experimentally for their possible application in optoelectronic devices.

Acknowledgement: DPR acknowledges Beijing Computational Science Research Center (Beijing, People's Republic of China) research fellowship and Dr. S. Rayaprol (rayaprol@gmail.com) UGC-DAE Consortium for Scientific Research BARC, Trombay (Mumbai, India) for valuable discussions and suggestions, RKT a research grant from UGC (New Delhi, India).

References

[1] C.M.I. Okoye. Eur. Phys. J. B, **39**, 5 (2004).
[2] D. Heciri, L. Beldi, S. Drablia, H. Meradji, N.E. Derradji, H. Belkhir, B. Bouhafs. Comp. Mater. Sci., **38**, 609 (2007).
[3] I. Khan, I Ahmad, D. Zhang, H.A. Rahnamaye, C.J. Asadabadi. J. Phys. Chem. Sol. **74**, 181 (2013).
[4] L. Guo, Ge Hu, S. Zhang, W. Feng, Z. Zhang. J. Alloys Comp., **561**, 16 (2013).
[5] J.C. Phillips, Van Vachten. Phys. Rev. Lett., **23**, 1115 (1969).
[6] B. Bouhafs, H. Aourag, M. Ferhat, M. Certier. J. Phys: Condens. Matter, **12**, 5655 (2000).
[7] D.J. Stukel. Phys. Rev B, **2**, 1852 (1970).
[8] R.L. Sarkar, S. Chatterjee. J. Phys. C, **10**, 57 (1977).
[9] M.G. Diaz, P.R. Hernandez, A. Munoz. Phys. Rev. B, **55**, 14 043 (1997).
[10] A. Munoz, P.R. Hernandez, A. Mujica. Phys. Sol., **198**, 439 (1996).
[11] G. Kalpana, G. Pari, A. Mookerjee, A. K. Bhattacharyya. Int. J. Mod. Phys. B, **12**, 1975 (1998).
[12] A. Fleszar, W. Hanke. Phys. Rev. B, **62**, 2466 (2000).
[13] S. Doyen-Lang, O. Pages, L. Lang, J. Hugel. Phys. Status Solidi B, **229**, 563 (2002).
[14] W.M. Yim, J.B. Dismakes, E.J. Stofko, R.J. Paff. J. Phys. Chem. Sol., **33**, 501 (1972).
[15] J.A. Vechten. Phys. Rev., **187**, 1007 (1969).
[16] A. Waag, F. Fischer, H.J. Lugauer, Th. Litz, J. Laubender, U. Lunz, U. Zhender, W. Ossau, T. Gerhardt, M. Moller, G. Landwehr, J. Appl. Phys., **80**, 792 (1996).
[17] J.P. Perdew, K. Burke, M. Ernzerhof. Phys. Rev. Lett., **77**, 3865 (1996).
[18] F. Aryasetiawan, O. Gunnarssson. Rep. Progr. Phys., **61**, 237 (1998).
[19] L.J. Sham, M. Schluter. Phys. Rev. Lett., **51**, 1888 (1983).
[20] A.D. Becke, M.R. Roussel. Phys. Rev. A, **39**, 3761 (1989).
[21] F. Tran, P. Blaha. Phys. Rev. Lett., **102**, 226 401 (2009).
[22] D. Koller, F. Tran, P. Blaha. Phys. Rev. B, **83**, 195 134 (2011).
[23] M. Yousaf, M.A. Saeed, R. Ahmed, M.M. Alsardia, A. Radzi, A. Shaari. Commun. Theor. Phys., **58** 777 (2012).
[24] R.B. Araujo, J.S. de Almeida, A.F. da Silva. J. Appl. Phys., **114**, 183 702 (2013).
[25] S.D. Guo, B.G. Liu. Europhys. Lett., **93**, 47 006 (2011).
[26] W. Al-Sawai, H. Lin, R.S. Markiewicz, L.A. Wray, Y. Xia, S.Y. Xu, M.Z. Hasan, A. Bansil. Phys. Rev. B, **82**, 125 208 (2010).
[27] P. Blaha, K. Schwarz, G.K.H. Madsen, D. Kvasnicka, J. Luitz, K. Schwarz. *An Augmented Plane Wave plus Local Orbitals Program for Calculating Crystal Properties.* Wien2K User's Guide, Techn. Universitat Wien (Wien, 2008).
[28] F.D. Murnaghan. Proc. Natl. Acad. Sci. USA, **30**, 244 (1944).
[29] S.H. Wei, A. Zunger. Phys. Rev. B, **53**, R10457 (1996).
[30] R. Khenata et al. Sol. St. Electron., **50**, 1382 (2006).
[31] I. Ajmad, B. Amin, M. Maqbool, S. Muhammad, G. Murtaza, S. Ali, A. Noor. Chin. Phys. Lett., **29** (9), 097 102 (2012).
[32] B. Amin, I. Ahmad, M. Maqbool, S. Goumrisaid, R. Ahmad. J. Appl. Phys., **109**, 023 109 (2011).
[33] F. Wooten. *Optical Properties of Solids* (Academic Press, N.Y., 1972).
[34] M. Fox. *Optical Properties of Solids* (Oxford, Oxford University Press, 2001).
[35] D. Penn. Phys. Rev. B, **128**, 2093 (1962).
[36] C. Becker et al. *Proc. 23rd int. conf. on Physics of Semiconductor* (Berlin–Singapore, World Scientific, 1996).
[37] J. Geurts et al. *Proc. 24th int. conf. on Physics of Semiconductor* (Singapore–Jerusalam, World Scientific, 1998).
[38] V.T. Vergaard, J.W. Hutshinson, J. Am. Ceram. Soc., **71**, 157 (1988).
[39] B. Mayer, H. Anton, E. Bott, M. Methfessel, J. Stricht, P.C. Schmidt. Intermettalics, **11**, 23 (2003).
[40] W. Voigt. *Lehrburch der Kristallphysik* (Teubner, Leipzig, 1928).
[41] A. Reuss, Z. Angew. Math. Mech., **9**, 49 (1929).
[42] W.A. Harisson. *Electronic Structures and Properties of solids* (Dover, N.Y., 1989).
[43] P.H. Mott, J.R. Dorgan, C.M. Roland. J. Sound and Vibrations, **312**, 572 (2008).
[44] V.V. Bannikov, I.R. Shein, A.L. Ivanovskii. Phys. Status Solidi. Rapid Res. Lett., **3**, 89 (2007).

[45] I.N. Frantsevich, F.F. Voronov, S.A. Bokuta. *Elastic Constants and Elastic Moduli of Metals and Insulators Handbook*, ed. by I.N. Frantsevich (Naukova Dumka, Kiev, 1983) p. 60.
[46] S.F. Pugh. Philos. Mag., **45**, 823 (1954).
[47] Xing-Qiu Chen, Haiyang Niu, Dianzhong Li, Yiyi Li. Intermetallics, **19**, 1275 (2011).
[48] J.J. Gilman. Hardness-a Strength Miroprobe, Chap. 4 of The Science of Hardness Testing and Its research Applications, eds J.H. Westbrook, H. Conrad (Ohio, USA, American Society of Metal, Metal Park, 1973).
[49] D.G. Pettifor. Mater. Sci. Technol., **8**, 345 (1992).
[50] P.F. Yuan, Z.J. Ding. Physica B, **403**, 1996 (2008).
[51] A. Bouhemadou, R. Khanate, M. Kharoubi, T. Seddik, A.H. Reshak, Y.A. Douri. Comput. Mater. Sci., **45**, 474 (2009).
[52] C. Narayana, V.J. Nesamony, A. Ruoff. Phys. Rev. B, **56**, 14 338 (1997).
[53] F.E.H. Hassan, H. Akbarzadeh. Comput. Mater. Sci., **35**, 423 (2006).
[54] H. Luo, K. Chandehari, R.G. Green, A. Ruoff, S.S. Trailand, F.J. Di Salvo. Phys. Rev. B, **2**, 1852 (1970).
[55] J.R. Christman. *Fundamentals of Solid State Physics* (Wiley, N. Y., 1988).
[56] O.L. Anderson. J. Phys. Chem. Sol., **24**, 909 (1963).
[57] E. Schreibe, O.L. Anderson, N. Soga. *Elastic Constants and their Measurements* (Mc Graw-Hill, N. Y., 1973).

Редактор Т.А. Полянская